



**Tailoring Non-fullerene Acceptors by Selenium-incorporated  
Heterocycles for Organic Solar Cells with over 16%  
Efficiency**

Journal:	<i>Journal of Materials Chemistry A</i>
Manuscript ID	TA-COM-07-2020-006658.R1
Article Type:	Communication
Date Submitted by the Author:	04-Sep-2020
Complete List of Authors:	<p>Yu, Han; The Hong Kong University of Science and Technology, Chemistry</p> <p>Qi, Zhenyu; Hong Kong University of Science and Technology, Chemistry</p> <p>Zhang, Jianquan; Hong Kong University of Science and Technology</p> <p>Wang, Zhen; North Carolina State University, Physics</p> <p>Sun, Rui; The Institute for Advanced Studies, Wuhan University,</p> <p>Chang, Yuan; Hong Kong University of Science and Technology, Chemistry</p> <p>sun, huiliang; Southern University of Science and Technology</p> <p>Zhou, Wentao; Hong Kong University of Science and Technology</p> <p>Min, Jie; The Institute for Advanced Studies, Wuhan University,</p> <p>Ade, Harald; North Carolina State University, Physics</p> <p>Yan, He; The Hong Kong University of Science and Technology, Department of Chemistry</p>

## Tailoring Non-fullerene Acceptors by Selenium-incorporated Heterocycles for Organic Solar Cells with over 16% Efficiency

Han Yu,<sup>§,⊥</sup> Zhenyu Qi,<sup>§,⊥</sup> Jianquan Zhang,<sup>§, ‡, \*</sup> Zhen Wang,<sup>#</sup> Rui Sun,<sup>&</sup> Yuan Chang,<sup>§</sup> Huiliang Sun,<sup>‡</sup> Wentao Zhou,<sup>§</sup> Jie Min,<sup>&</sup> Harald Ade,<sup>#, \*</sup> He Yan<sup>§, ‡, Δ, \*</sup>

<sup>§</sup> Department of Chemistry and Hong Kong Branch of Chinese National Engineering Research Center for Tissue Restoration and Reconstruction, Hong Kong University of Science and Technology, Clear Water Bay, Kowloon, Hong Kong

<sup>‡</sup> Hong Kong University of Science and Technology-Shenzhen Research Institute, No. 9, Yuexing 1st RD, Hi-tech Park, Nanshan, Shenzhen 518057, China

<sup>#</sup> Department of Physics and Organic and Carbon Electronics Laboratories (ORaCEL), North Carolina State University, Raleigh, NC 27695, United States

<sup>&</sup> The Institute for Advanced Studies, Wuhan University, Wuhan 430072, China

<sup>Δ</sup> Institute of Polymer Optoelectronic Materials and Devices, State Key Laboratory of Luminescent Materials and Devices, South China University of Technology, Guangzhou 510640, China

<sup>⊥</sup>These authors contributed equally to this work.

**Abstract**

Small molecular acceptors (SMAs) have gained extensive research attention as they offer many attractive features and enable highly efficient organic solar cells (OSCs) that cannot be achieved using fullerene acceptors. Recently, a new SMA named Y6 was reported, yielding high-performance OSCs with efficiencies of 15.7%. This report has inspired the OSC community to study the structure-property relationship and further modify this important class of materials. In this work, we used the selenium (Se) substitution strategy and developed two new Y6-type SMAs to study the effect of Se atoms on material properties and device performances. It is found that the introduction of Se atoms can red-shift the absorption spectra and enhance the aggregation of the resulting SMAs. Interestingly, the variations in the substitution positions of Se atoms induces different intramolecular charge transfer within the SMAs. Se substitution at the benzothiadiazole ring is more effective than those at the thienothiophene rings, leading to the increased short-circuit current density ( $J_{SC}$ ) and higher efficiencies of over 16%. This contribution suggests that appropriate Se substitution is a promising method for optimizing absorption and aggregation of Y6-type SMAs, thus enhancing their OSC performances.

## Introduction

In recent years, organic solar cells (OSCs) have achieved great success and been considered as one of the promising replacement of the traditional inorganic solar cells due to their multiple advantages, such as low cost, portability, and mechanical flexibility.<sup>1-7</sup> Although fullerene derivatives have been utilized as electron acceptors in traditional OSCs, they suffer from insufficient absorption, fixed chemical structure and poor photochemical and thermal stability. Enormous efforts have been contributed to developing non-fullerene electron acceptors, particularly small molecular acceptors (SMAs).<sup>8-18</sup> Benefitting from their easily tunable chemical structures and optoelectronic properties, power conversion efficiencies (PCEs) of over 16% have been achieved by SMA-based OSC devices, demonstrating their great potential in commercial applications.<sup>19-27</sup> Recently, an efficient SMA named Y6, featuring an A'-DAD-A' structure, was reported to yield high-performance OSCs with PCEs of 15.7% *via* delicate molecular design and device optimization.<sup>28-30</sup>

Despite the great progress made in Y6-based OSCs,<sup>41-45</sup> the trade-off among the open-circuit voltage ( $V_{OC}$ ), short-circuit current density ( $J_{SC}$ ) and fill factor (FF) remains a challenge that limits further improvement of device efficiencies. Typically, regulation of the central molecular core is able to tune the intramolecular charge transfer (ICT) strength to improve the  $J_{SC}$  of OSC devices.<sup>46-51</sup> Sulfur-based heterocycles, such as thiophene and benzothiadiazole, are widely utilized as building blocks to construct conjugated molecules in the OSC field, due to their synthetic flexibility and excellent optoelectronic properties. Structurally similar to sulfur-based heterocycles, selenium-substituted analogs have also attracted considerable attention in the molecular design of conjugated polymers and small molecules.<sup>52-57</sup> Compared to sulfur, selenium has a larger atomic radius and d-orbitals that are more polarizable. As a result, strong intermolecular Se $\cdots$ Se non-covalent interactions are induced, facilitating well-aligned solid-state packing and thus charge carrier mobility.<sup>58-63</sup> In addition, the  $\pi$ -electrons in

selenium-substituted heterocycles tend to adopt a more quinoidal character, showing enhanced planarity and leading to smaller optical bandgaps and red-shifted absorption spectra.<sup>64-68</sup> Therefore, selenium-substituted OSC materials usually yield higher  $J_{SC}$  relative to their sulfur-based analogs. Despite these advantageous properties, few systematic studies have been thoroughly carried out on heterocycle engineering of SMAs by replacing sulfur with selenium, especially from the perspective of obtaining high-performance OSCs with over 15% efficiency.

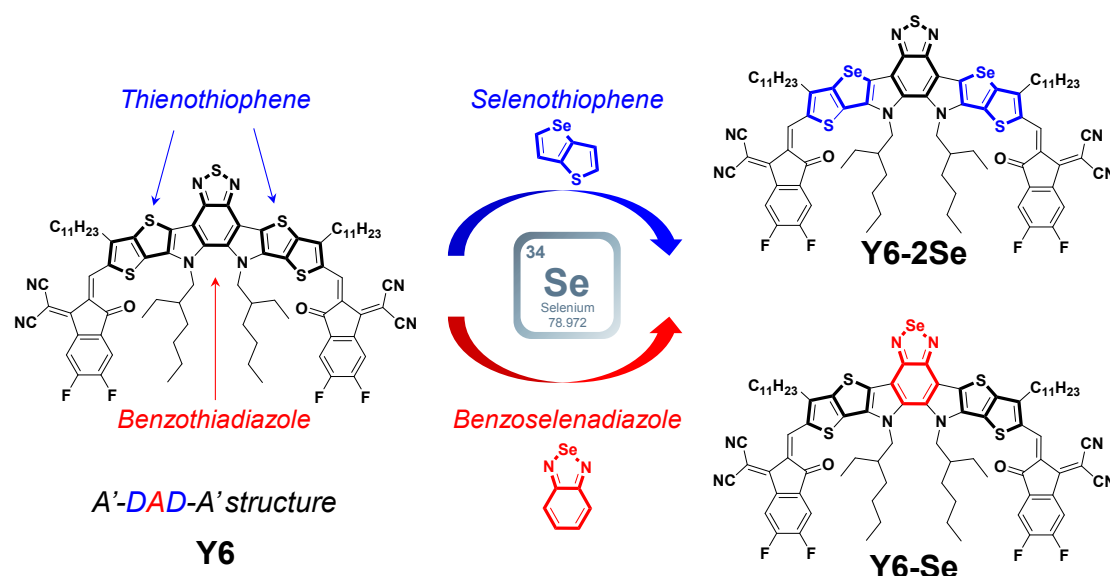
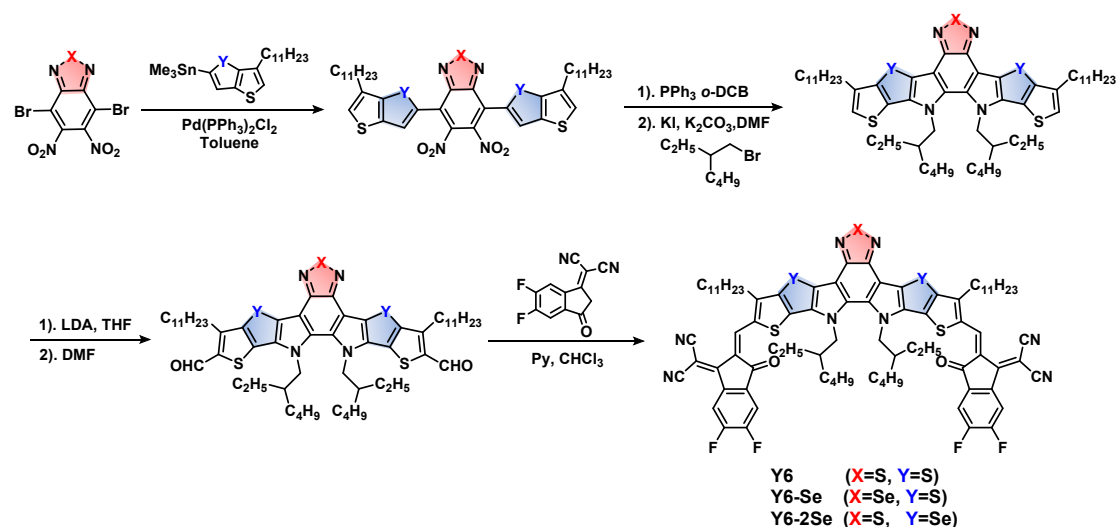


**Figure 1.** Chemical structure of Y6 and two Se-substituted derivatives, Y6-Se and Y6-2Se.

In this contribution, we, for the first time, examined the effect of selenium substitution in constructing A'-DAD-A'-type electron acceptors for OSC operations. Two selenium-substituted Y6 derivatives named Y6-Se and Y6-2Se were synthesized and systematically studied (**Figure 1**), with two molecules differing in the substitution positions of the central backbone (i.e., sulfur at benzothiadiazole and sulfur at thienothiophene). When blended with the donor polymer PM6, both devices based on selenium-substituted SMAs exhibited similar  $V_{OC}$  of  $\sim 0.83$  V to those based on Y6.

However, both selenium-substituted acceptors displayed bathochromic absorption caused by the stronger ICT effect. The Y6-Se-based devices showed enhanced  $J_{SC}$  and FF compared with Y6- and Y6-2Se-based ones, yielding the highest PCE of 16.02%. Morphological studies elucidated that suitable nanoscale phase segregation is formed in PM6: Y6-Se blends, leading to more efficient charge dissociation and suppressed charge recombination, which contributes to the higher performances. Our work provides insights into the structure-performance relationship of the selenium-substituted Y6-type SMAs and demonstrates the promising applications of selenium-based derivatives for designing the active-layer materials for OSCs.

## Results and Discussions



**Scheme 1.** Synthetic route to Y6-Se and Y6-2Se.

The synthetic routes to Y6-Se and Y6-2Se, which are similar to that of Y6, are illustrated in **Scheme 1**. To begin with, 4,7-dibromo-5,6-dinitrobenzo[c][1,2,5]selenadiazole or 4,7-dibromo-5,6-dinitrobenzo[c][1,2,5]thiadiazole underwent Stille cross-coupling reactions with trimethyl(3-undecylthieno[3,2-b]thiophen-5-yl)stannane and trimethyl(3-undecylselenopheno[3,2-b]thiophen-5-yl)stannane, respectively. The resultant

coupling products containing one or two selenium atoms were subsequently conducted to a three-step procedure of cyclization via  $\text{PPh}_3$  reduction, alkylation, and formylation through nucleophilic substitution to obtain the dialdehyde precursors. Finally, the dialdehyde intermediates were condensed with 2-(5,6-difluoro-3-oxo-2,3-dihydro-1H-inden-1-ylidene) malononitrile (2F-IC) to yield Y6-Se and Y6-2Se through Knoevenagel reactions. All the intermediates and final products were clearly characterized by  $^1\text{H}$  NMR,  $^{13}\text{C}$  NMR and mass spectra, which are summarized in the Supporting Information. The thermal decomposition temperature ( $T_d$ ) of Y6-Se and Y6-2Se is 227 °C and 337 °C by thermogravimetric analysis (TGA, at 5% weight loss, **Figure S1**) indicating that both molecules have good thermal stability and are thus suitable for OSC operation.

To explore the selenium-substitution effects of Y6-Se and Y6-2Se relative to Y6, density-functional theory (DFT) was utilized for theoretical calculations at the B3LYP/6-31(d,p) basis set to investigate the molecular geometries and frontier molecular orbitals. The undecyl chains on the thiophene units and 2-ethylhexyl branched chains on the pyrrole units were replaced by methyl groups and 2-methylpropyl groups in order to simplify the calculations, respectively. As presented in **Figure 2a–c**, both Y6-Se and Y6-2Se exhibit twisted helical molecular geometry that is similar to Y6, indicating that the introduction of selenium does not alter the geometry despite its larger atom size. As displayed in **Figure 2d–f**, the HOMO and LUMO of all three SMAs are distributed through the entire molecular backbone, implying that Se can also form good conjugation as S does. It can be observed that after the incorporation of Se atoms, the HOMO levels upshifted while the LUMO levels showed little changes, leading to narrower bandgaps of Y6-Se and Y6-2Se. This can be attributed to the enhanced ICT after selenium substitution (**Figure 2g–i**), which was elucidated by the dipole moment calculations of the half molecule skeleton (8.00 D for Y6, 8.57 D for Y6-Se and 8.33 D for Y6-2Se, respectively). More interestingly, the selenium

substitution at the benzothiadiazole moiety can achieve stronger ICT than that at the thienothiophene units despite the fewer selenium atoms in Y6-Se.

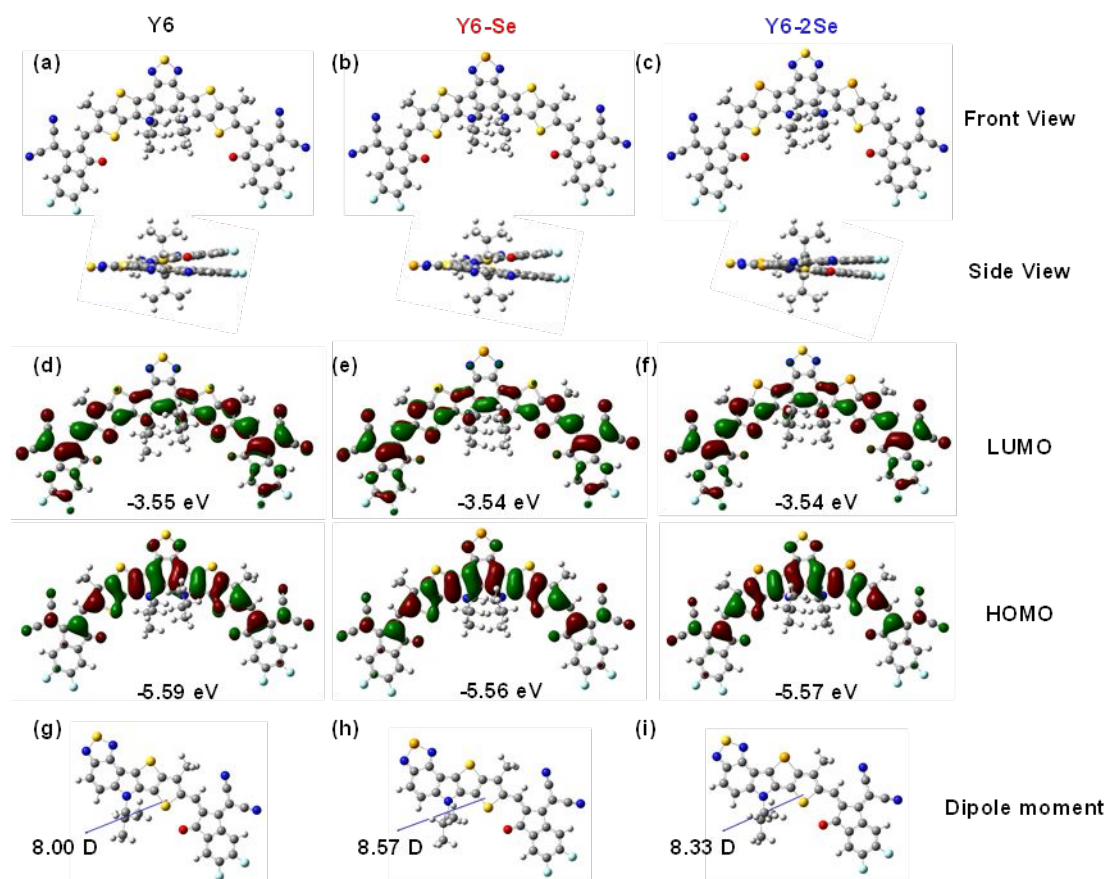


**Figure 2.** Optimized molecular geometry of (a) Y6, (b) Y6-Se and (c) Y6-2Se; frontier molecular orbitals of (d) Y6, (e) Y6-Se and (f) Y6-2Se; Dipole moment of (g) Y6, (h) Y6-Se and (i) Y6-2Se calculated at the B3LYP/6-31(d,p) level.

As illustrated in **Figure 3a**, the solution UV-Vis absorption spectra of Y6, Y6-Se and Y6-2Se were recorded with a concentration of  $1 \times 10^{-5}$  M. While Y6 shows a major absorption peak located at 729 nm with a maximum extinction coefficient ( $\alpha_{\max, \text{sol}}$ ) of  $1.52 \times 10^5 \text{ M}^{-1} \text{ cm}^{-1}$ , both selenium-substituted Y6-Se and Y6-2Se exhibit bathochromic absorption peaks located at 745 nm with extinction coefficients of  $1.53 \times 10^5$  and  $1.60 \times 10^5 \text{ M}^{-1} \text{ cm}^{-1}$ , respectively. These bathochromic peaks are owing to the stronger

ICT from the selenium-substituted cores to the end groups as supported by the DFT calculations above. And interestingly, the ICT effect seems comparable between Y6-Se and Y6-2Se in solution state despite the different number and the substituted positions of Se atoms. In thin-film state, all SMAs exhibit bathochromic absorption relative to their solution state with the onsets of 912, 946 and 922 nm for Y6, Y6-Se and Y6-2Se, corresponding to the optical bandgaps ( $E_g$ ) of 1.36, 1.31 and 1.34 eV, respectively. As a result, the blend films of SMAs with PM6, covering the range of 300-900 nm in the solar spectrum (**Figure S2**). It is noteworthy that Y6-Se shows the largest red-shift (148 nm) of its absorption spectra from solution to thin-film state when compared with Y6 (129 nm) and Y6-2Se (124 nm). A plausible reason for this phenomenon is that the selenium substitution at the central benzothiadiazole moiety of Y6 enables more compact molecular stacking in solid state induced by strong Se $\cdots$ Se non-covalent interactions. Therefore, it is anticipated that Y6-Se should have better photon-harvesting ability as well as charge carrier transport relative to the other two SMAs.

In terms of the electrochemical properties, cyclic voltammetry (CV, **Figure 3c**) was carried out in film state to estimate the energy levels of the SMAs by using ferrocene/ferrocenium (-4.8 eV) as the external standard. As shown in **Figure 3d**, while showing comparable LUMO levels of  $\sim$ -3.84 eV, Y6-Se and Y6-2Se have slightly upshifted HOMO levels of -5.55 eV and -5.58 eV, respectively, relative to Y6 (-5.61 eV), which shows the same trend as the calculation results above. Hence, the narrower electrochemical band gaps of Y6-Se and Y6-2Se are consistent with their optical bandgap. In addition, as the HOMO levels of Y6-Se and Y6-2Se approach to that of PM6 (-5.52 eV), the energetic offsets between PM6 and both selenium-substituted SMAs should be smaller, and the voltage loss ( $V_{\text{loss}}$ ) of the devices are expected to be decreased.

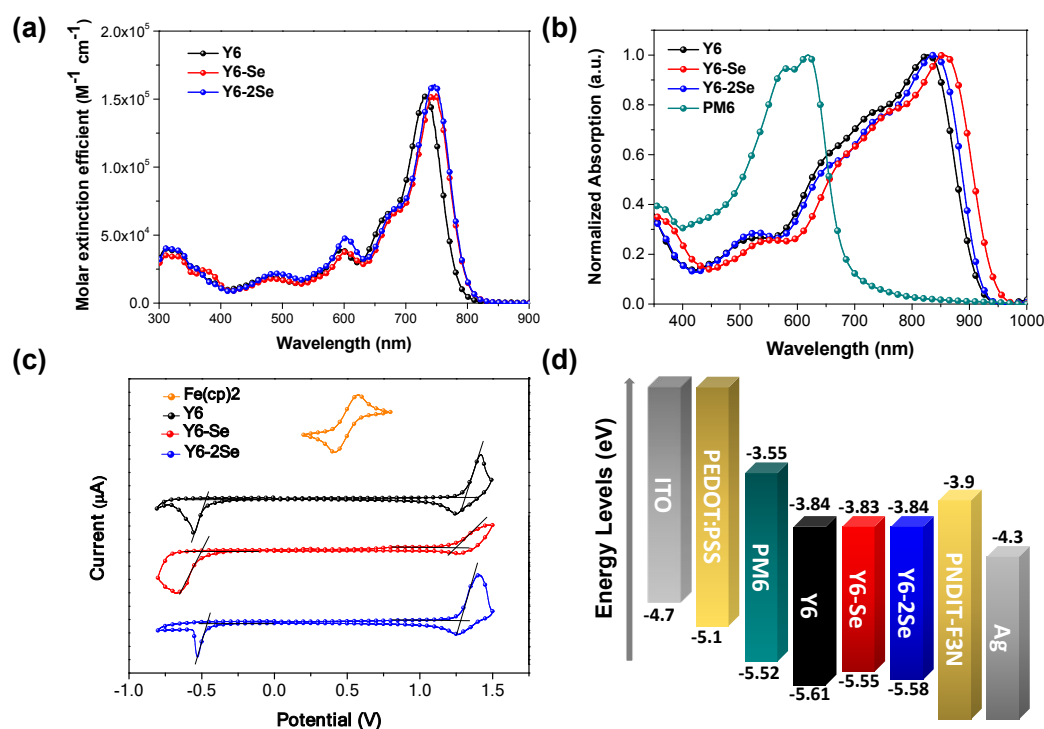


**Figure 3.** (a) UV-Vis absorption spectra of Y6, Y6-Se and Y6-2Se in dilute chloroform solution (concentration:  $1.0 \times 10^{-5}$  M). (b) Normalized UV-Vis absorption spectra of PM6, Y6, Y6-Se and Y6-2Se in thin-film state. (c) Cyclic voltammetry curves of Y6, Y6-Se and Y6-2Se. (d) Architecture and energy alignment of the bulk heterojunction devices.

**Table 1.** Optical and electrochemical properties of Y6, Y6-Se and Y6-2Se.

	$T_d$ [°C]	$\lambda_{\max, \text{sol}}$ [nm]	$\lambda_{\text{onset, sol}}$ [nm]	$\alpha_{\max, \text{sol}}$ [M <sup>-1</sup> cm <sup>-1</sup> ]	$\lambda_{\text{onset, film}}$ [nm]	$E_g^a$ [eV]	LUMO <sup>b</sup> [eV]	HOMO <sup>b</sup> [eV]
<b>Y6</b>	213	729	783	$1.52 \times 10^5$	912	1.36	-3.84	-5.61
<b>Y6-Se</b>	227	745	798	$1.53 \times 10^5$	946	1.31	-3.83	-5.55
<b>Y6-2Se</b>	337	745	798	$1.60 \times 10^5$	922	1.34	-3.84	-5.58

<sup>a</sup> calculated from the absorption onset of the films.

<sup>b</sup> estimated from the reduction/oxidation onset of the CV curves.

**Table 2.** Photovoltaic parameters of the solar cell devices based on PM6:Y6, PM6:Y6-Se and PM6:Y6-2Se with the normal structure under the illumination of 100 mW/cm<sup>2</sup>.

Material combinations	$V_{OC}$ (V)	$J_{SC}$ (mA/cm <sup>2</sup> )	FF (%)	PCE (%)	$\mu_h, \mu_e$ (cm <sup>2</sup> /Vs)
PM6:Y6	0.83±0.01	24.80±0.47	74±1	15.35±0.20 (15.67)	4.86×10 <sup>-4</sup> , 4.18×10 <sup>-4</sup>
PM6:Y6-Se	0.82±0.01	25.47±0.33	75±1	15.82±0.14 (16.02)	5.07×10 <sup>-4</sup> , 4.78×10 <sup>-4</sup>
PM6:Y6-2Se	0.83±0.01	24.32±0.49	70±1	14.62±0.15 (14.94)	4.19×10 <sup>-4</sup> , 3.25×10 <sup>-4</sup>

<sup>a</sup> Average values from 20 devices with the highest values shown in parentheses.

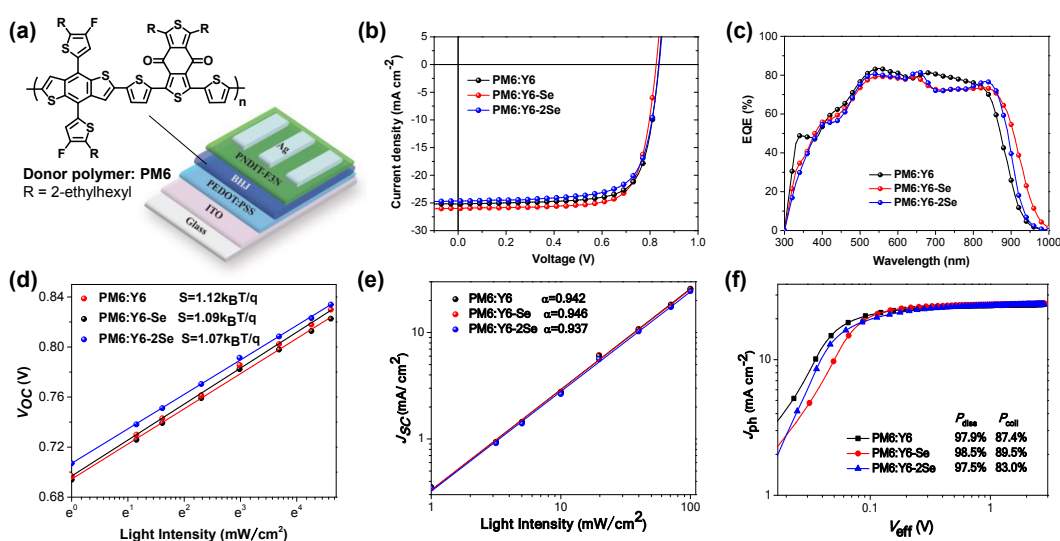


**Figure 4.** (a) Device architecture, (b)  $J$ - $V$  characteristics, (c) EQE spectra, (d) Light-intensity-dependent  $V_{OC}$  plots and (e) light-intensity-dependent  $J_{SC}$  plots and (f) photocurrent versus effective voltage plots of the PM6:Y6, PM6:Y6-Se and PM6:Y6-2Se devices.

To investigate the photovoltaic performances of selenium-substituted SMAs, OSCs were fabricated with the conventional device structure of ITO/PEDOT:PSS/PM6:SMA/PNDIT-F3N/Ag (**Figure 4a**). The optimized devices photovoltaic parameters are summarized in **Table 2** and the current density versus voltage ( $J-V$ ) curves of the PM6:Y6, PM6:Y6-Se and PM6:Y6-2Se devices are shown in **Figure 4b**. All three material systems generated similar  $V_{OC}$  of 0.83, 0.82 and 0.84 V for the PM6:Y6, PM6:Y6-Se and PM6:Y6-2Se devices, respectively, which can be ascribed to their similar LUMO levels. Although the  $V_{OC}$  is comparable, three devices exhibit noticeable differences in  $J_{SC}$  and FF with various type of selenium substitution. The  $J_{SC}$  of the Y6-Se-based devices is higher than that of Y6-based ones (25.99 vs. 25.18 mA/cm<sup>2</sup>) due to the extended absorption range. Together with a slightly higher FF of 75%, the PM6:Y6-Se devices achieved a PCE of 16.02%, which outperformed that of the PM6:Y6 ones (15.67%). Note that such an efficiency of over 16% obtained by Y6-Se is the highest value among the reported selenium-substituted SMAs. In contrast, the Y6-2Se-based devices yielded a lower  $J_{SC}$  of 24.65 mA/cm<sup>2</sup> despite its red-shifted absorption relative to Y6, and a lower FF of 72%, resulting in an inferior PCE of 14.94%.

External quantum efficiency (EQE) spectra were recorded based on the three blends to reveal the reason for the differences in  $J_{SC}$  among these devices. As displayed in **Figure 4c**, the light response range of all EQE curves is consistent with their blend film absorption, where the highest EQE values are ~80% for all the three devices. The integrated  $J_{SC}$  calculated from the corresponding EQE spectra are 24.81, 25.28 and 24.61 mA/cm<sup>2</sup> for Y6, Y6-Se and Y6-2Se-based devices, respectively, which are in good agreement with the values attained from the  $J-V$  characteristics. Clearly, the EQE results reveal that the increase of  $J_{SC}$  from Y6 to Y6-Se is caused by the extended EQE contribution in the range of 840-1000 nm. Although the EQE spectrum of the Y6-2Se-

based device also exhibits extended photon response, it cannot compensate the loss caused by the spectrum defect from 660 nm to 810 nm compared with the Y6-based one, thus leading to a lower  $J_{SC}$  of the devices. The series resistances ( $R_S$ ) attained from the  $J-V$  curve of the three optimal devices (Table. S1) are 5.2, 3.9 and 6.0  $\Omega \text{ cm}^2$  for the PM6:Y6, PM6:Y6-Se and PM6:Y6-2Se devices, respectively. Additionally, the shunt resistance ( $R_{Sh}$ ) are determined to be 2.0, 2.6 and 1.9  $\text{k}\Omega \text{ cm}^2$  for the PM6:Y6, PM6:Y6-Se and PM6:Y6-2Se devices, respectively. The series resistances under the dark conditions (**Fig. S3**) exhibit the same trend as those calculated from the  $J-V$  curves. The reduced  $R_S$  and increased  $R_{Sh}$  should be one of the reasons for the increased FF in the optimized PM6:Y6-Se devices.<sup>69</sup>

Moreover, charge dissociation process based on three blend films were set to investigate through photoluminescence quenching experiments. Lasers with the wavelengths of 514 nm and 785 nm were selected to excite PM6 and the SMAs, respectively. As exhibited in **Figure S3**, more red-shifted photoluminescence peaks of Y6-Se can be attributed to the better molecular stacking in solid state, which is consistent with the more bathochromic absorption peak in solid state as well. The quenching efficiency of the PM6:Y6-2Se blend film relative to the pristine PM6 film (77.2%) is the lowest among three blend films (81.4% for PM6:Y6 and 84.4% for PM6:Y6-Se). Similar situations were discovered when comparing the blends and the pristine SMA-based films, where the quenching efficiencies of the Y6, Y6-Se and Y6-2Se-based systems were estimated to be 89.9%, 91.9% and 84.1%, respectively. Consequently, the photoluminescence quenching experiments reveal that the Y6-Se based blend shows both more efficient electron and hole transfer processes than the other two systems, leading to the higher  $J_{SC}$  of the devices.

The notable changes in the  $J_{SC}$  and FF among the three SMA-based devices were further investigated by charge recombination experiments. **Figure 4d-e** illustrate the results of

the light-intensity-dependent  $V_{OC}$  and  $J_{SC}$  measurements. **Figure 4d** describes the semi-logarithmic plots of the light-intensity-dependent  $V_{OC}$  experiments based on these three systems. The slopes extracted from the plots are  $1.12 k_B T/q$ ,  $1.09 k_B T/q$  and  $1.07 k_B T/q$  for the PM6:Y6, PM6:Y6-Se and PM6:Y6-2Se devices, respectively, where  $k_B$  is the Boltzmann constant,  $T$  is the absolute temperature and  $q$  is the elementary charge. These slope values close to  $k_B T/q$  suggest that the dominant recombination mechanism should be bimolecular recombination for all the devices. Furthermore, the relationship between  $J_{SC}$  and light intensity ( $P$ ), which can be described as  $J_{SC} \propto P^\alpha$ , was used to analyze the bimolecular recombination in these devices (**Figure 4e**). The  $\alpha$  values were determined to be 0.942, 0.946 and 0.937 for of the Y6, Y6-Se and Y6-2Se-based devices, respectively. This implies that the Y6 and Y6-Se-based devices present relatively weak bimolecular recombination and balanced charge transport (as will be discussed below). Therefore, these light-intensity-dependent experiments demonstrate effectively suppressed charge recombination in the Y6 and Y6-Se-based devices, which can partially explain their higher  $J_{SC}$  along with FF than the Y6-2Se one.

Furthermore, charge separation of three blend films was examined by the method of charge dissociation probability  $P(E,T)$  as displayed in **Figure 4f**. We plotted the photocurrent density  $J_{ph}$  (defined by  $J_L - J_D$ , where  $J_L$  and  $J_D$  are light and dark current density) against the effective voltage  $V_{eff}$  (defined by  $V_{cor} - V_0$ , where  $V_{cor}$  is the applied voltage corrected for the series resistance,  $V_0$  is the voltage when  $J_{ph} = 0$ ) in logarithmic scale.<sup>70</sup> Then, the  $P(E,T)$  can be calculated according to the equation of  $J/J_{sat}$ , where  $J_{sat}$  is the photocurrent density that reaches saturation at high reverse voltage, suggesting that all the photogenerated excitons are dissociated into free charges and swept out. Under short-circuit condition, the  $P(E,T)$  values are 97.9%, 98.5% and 97.5%, while under maximum power output conditions, the  $P(E,T)$  values are 87.4%, 89.5% and 83.0% for PM6:Y6, PM6:Y6-Se and PM6:Y6-2Se respectively. Therefore, the highest  $P(E,T)$

values of the PM6:Y6-Se blend under both short-circuit and maximum power output conditions should explain the increase of  $J_{SC}$  of the device.

To understand the molecular packing of Y6, Y6-Se and Y6-2Se, grazing incidence wide-angle X-ray scattering (GIWAXS) experiments were carried out for both pristine and blend films. The two-dimensional GIWAXS patterns are shown in **Figure 5a-f**, and the corresponding one-dimensional line-cut scattering profiles in the in-plane (dash line) and out-of-plane (solid line) directions of the pristine and blend films are displayed in **Figure 5g**. The (010) peaks of the pristine Y6, Y6-Se and Y6-2Se films are positioned at 1.79, 1.80 and 1.88  $\text{\AA}^{-1}$ , the corresponding  $\pi$ - $\pi$  stacking distances are calculated to be 3.51, 3.48 and 3.35  $\text{\AA}$ , respectively. The selenium-substituted SMAs indeed have shorter  $\pi$ - $\pi$  stacking distances than Y6. After blended with the donor, all combinations show remarkable face-on orientation with the  $\pi$ - $\pi$  stacking peaks in the out of plane direction positioned at 1.76  $\text{\AA}^{-1}$ , 1.76  $\text{\AA}^{-1}$  and 1.75  $\text{\AA}^{-1}$ , respectively, and strong (100) peaks in the in-plane direction. The (010) coherence lengths of three SMA blends were extracted to be 23.6, 26.8 and 22.8  $\text{\AA}$  when blended with PM6, respectively. Larger coherence length can lead to better charge transport, which is supported by electron mobility measurements (**Table 2**,  $4.18 \times 10^{-4} \text{ cm}^2/\text{Vs}$  for PM6:Y6,  $4.78 \times 10^{-4} \text{ cm}^2/\text{Vs}$  for PM6:Y6-Se and  $3.25 \times 10^{-4} \text{ cm}^2/\text{Vs}$  for PM6:Y6-2Se, respectively) evaluated by the space-charge-limited current (SCLC, **Figure S4**) method. As a result and in accordance with prior observations,<sup>71</sup> the PM6: Y6-Se device demonstrates higher charge mobilities and more balanced hole/electron charge transport compared to the other two SMA-based ones, accounting for the higher FF of the PM6: Y6-Se system.

Resonant soft X-ray scattering (RSoXS) techniques were utilized to estimate the nano-scale phase segregation of these three blends in order to understand distinct variations in charge dissociation and transport among three SMA-based systems.<sup>72-73</sup> **Figure 6a** displays the Lorentz-corrected RSoXS profiles of the PM6:Y6, PM6:Y6-Se and

PM6:Y6-2Se blend films attained at 283.8 eV. The long periods of the three blends were calculated to be 73.9, 84.9 and 65.4 nm for PM6:Y6, PM6:Y6-Se and PM6:Y6-2Se, respectively. In addition, the overall root-mean-square variation  $\sigma$  of the composition of the three blends were determined to be 0.89, 1.00 and 0.86 for PM6:Y6, PM6:Y6-Se and PM6:Y6-2Se, respectively. Higher  $\sigma$  can be directly linked to better FF.<sup>74</sup> The Y6-Se blend indeed shows not only better  $\pi$ - $\pi$  stacking but also higher domain purity, which could explain its better EQE response, photoluminescence quenching efficiency, as well as electron mobility mentioned above. Additionally, the surface roughness of the three blends is also illustrated by the atomic force microscopy (AFM, **Figure 6b-d**) images, where the Y6-Se-based blend shows smoother surface morphology (RMS=1.06 nm) than the other two SMA-based ones (1.13 nm for PM6:Y6 and 1.16 nm for PM6:Y6-2Se, respectively), leading to a better contact with electron-transporting layer and electrode and therefore efficient charge collection.

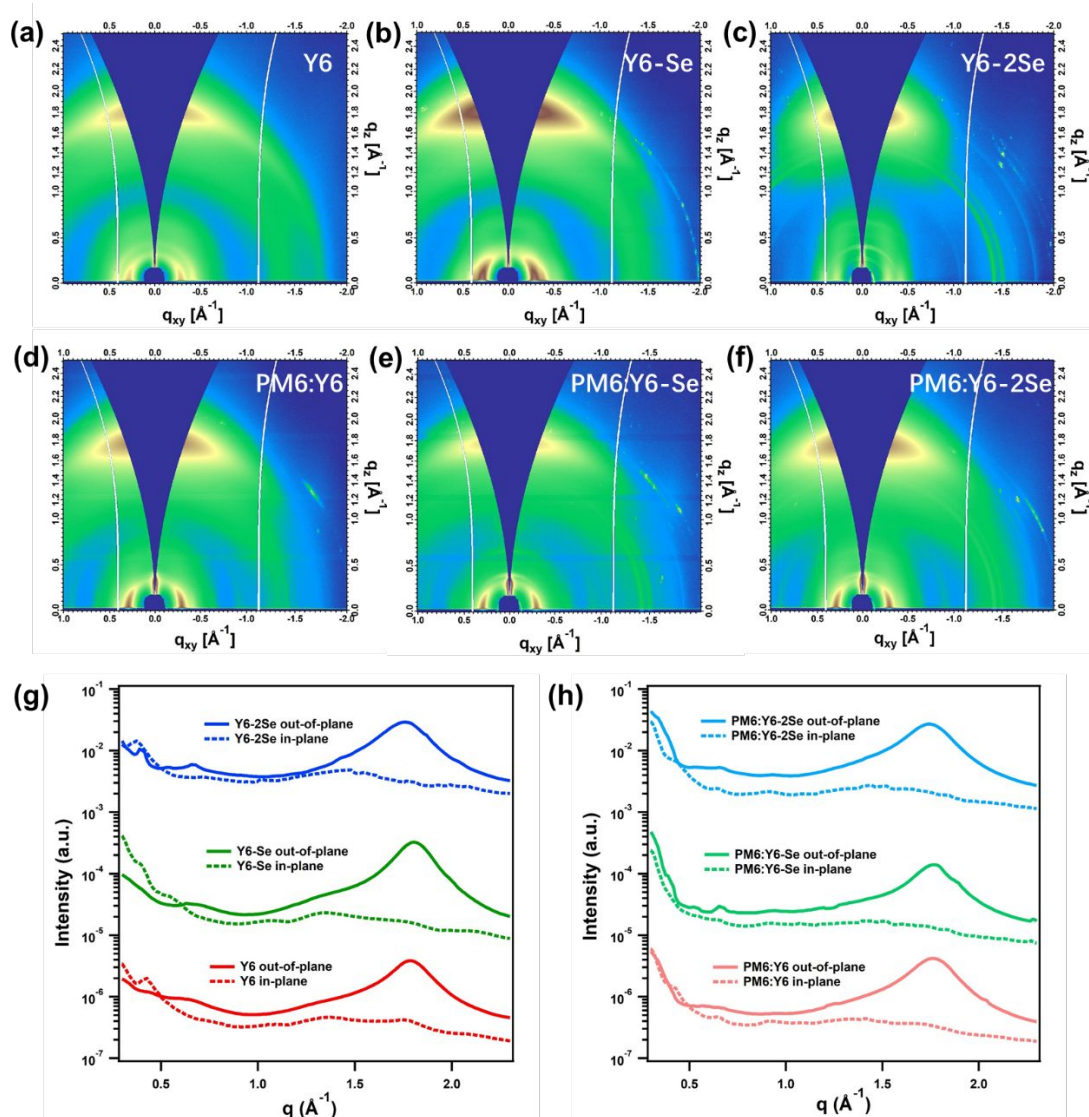


**Figure 5.** 2D GIWAXS patterns of (a) the pristine Y6 film, (b) the pristine Y6-Se film, (c) the pristine Y6-2Se film, (d) the PM6: Y6 blend film, (e) the PM6: Y6-Se blend film, (f) the PM6: Y6-2Se blend film, (g) the corresponding pristine and (h) the corresponding blend 1D GIWAXS profiles of the in-plane and out-of-plane directions.

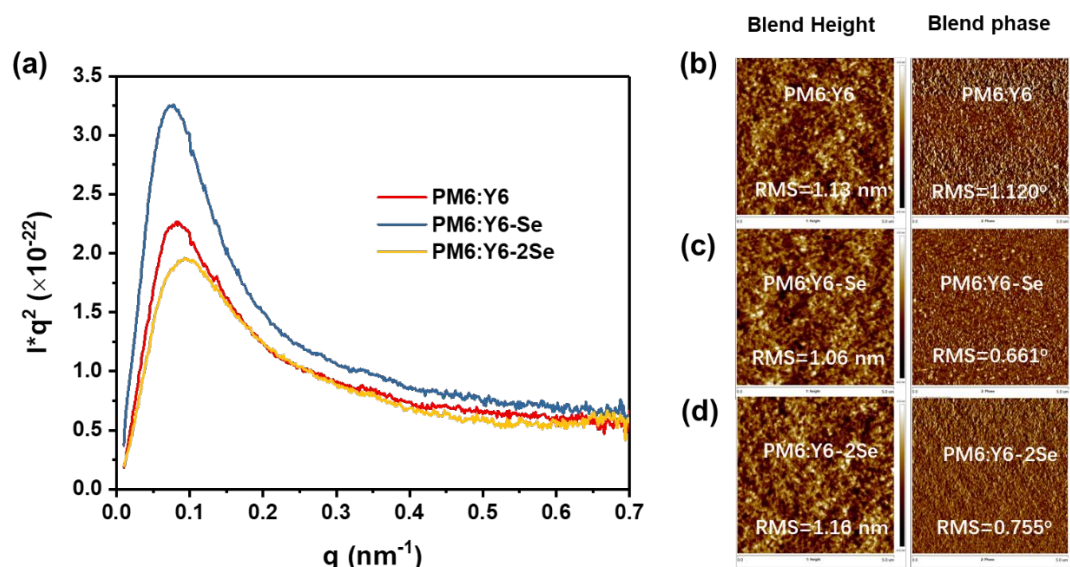


**Figure 6.** (a) Lorentz-corrected RSoXS profiles of the PM6:Y6, PM6:Y6-Se and PM6:Y6-2Se blend films acquired at 283.8 eV, the AFM height and phase images of (b) the PM6:Y6 blend film, (c) the PM6:Y6-Se blend film and (d) the PM6:Y6-2Se blend film.

To investigate the origins of the comparable  $V_{OC}$  among the three OSC systems, the detailed energy losses were investigated of the devices (**Figure 7** and **Table S6**). The  $V_{loss}$  (defined as  $V_{loss} = E_g/q - V_{OC}$ ) based on the PM6:Y6, PM6:Y6-Se and PM6:Y6-2Se combinations are calculated to be 0.58, 0.55 and 0.56 V, respectively, indicating that selenium substitutions can reduce the HOMO offset between PM6 and the SMAs and thus achieve low  $V_{loss}$ . Based on the detailed balance theory, the first part  $\Delta E_1$  ( $E_g - qV_{oc}^{SQ}$ ) from radiative recombination loss above the  $E_g$ , is inevitable for all types of solar cells,<sup>75</sup> and the three cases demonstrate almost identical  $\Delta E_1$  ( $\sim 0.25$  eV). The second part  $\Delta E_2$  ( $qV_{oc}^{SQ} - qV_{oc}^{rad}$ ) from radiative recombination loss depends on the absorption below the  $E_g$ , and Y6-Se-based device shows comparable  $\Delta E_2$  of 0.08 eV as those of the other two SMA-based ones (0.06 eV for PM6:Y6 and 0.07 eV for PM6:Y6-2Se).<sup>76-77</sup> As for the third part  $\Delta E_3$  (the non-radiative recombination loss) is attained through the following equation:  $\Delta E_3 = -kT \ln(EQE_{EL})$ . Due to the lower energy offset between PM6 and Y6-Se, it was found that Y6-Se-based device exhibits a higher  $EQE_{EL}$  than

those of the other two SMA-based devices (**Figure S6d-f**) and the corresponding  $\Delta E_3$  are calculated to be 0.24 eV, 0.22 eV and 0.24 eV, respectively. Based on these results and previous report, the small energy offset between donor and acceptor caused by selenium substitution can effectively suppress the charge-transfer (CT) state recombination through the hybridization of the local excited (LE) state and the CT state, resulting in reduced non-radiative loss.<sup>78</sup>

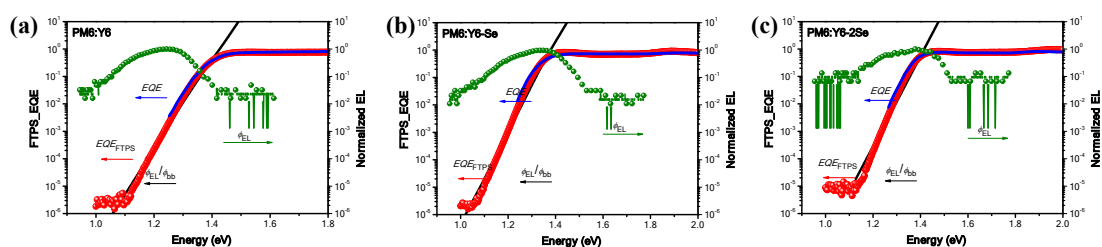


**Figure 7.** (a-c) Semi-logarithmic plots of normalized EL, measured EQE and EQE calculated by FTPS ( $\text{EQE}_{\text{FTPS}}$ ) as a function of energy for devices based on PM6:Y6 (a), PM6:Y6-Se (b), and PM6:Y6-2Se (c). The ratio of  $\varphi_{\text{EL}}/\varphi_{\text{bb}}$  was used to plot the EQE in the low-energy regime (black line), where  $\varphi_{\text{EL}}$  and  $\varphi_{\text{bb}}$  represent the emitted photon flux and the room-temperature blackbody photon flux, respectively. Of note is that  $\varphi_{\text{EL}}/\varphi_{\text{bb}}$  follows experimental  $\text{EQE}_{\text{FTPS}}$  faithfully at higher energies as expected from reciprocity.

## Conclusions

In conclusion, we designed and synthesized two selenium-substituted SMAs derived from Y6 for OSC fabrications. Because of the variations in the selenium-substituted positions on the electron-deficient central moiety, BFC-4F and YBOC-4F presented different absorption and optoelectronic properties. When blended with PTQ10, the comparisons in their blend film morphology indicated that the PM6:Y6-Se blend formed suitable phase separation, thus leading to a more efficient exciton dissociation, better charge transportation and lower extent of charge recombination. Consequently, the PM6:Y6-Se devices attained the highest PCE of 16.02% with a  $V_{\text{OC}}$  of 0.82 V, a

remarkably enhanced  $J_{SC}$  of 25.47 mA cm<sup>-2</sup>, and a smaller voltage loss of 0.49 V, which was superior to the PM6:Y6 (15.67%) and PM6:Y6-2Se ones (14.94%). Our work shed light on another structure-property-performance relationship of Y6-based SMAs and highlight the significance of appropriate substitution of selenium atoms in optimizing the absorption and aggregation properties of SMAs, and eventually enhancing OSC performances.

Further red-shifting the optical absorption of such SMAs to beyond 1000 nm would be of great research interest and importance. In this work, we examined two types of Se substitution on Y6. However, there are other possible Se-substitution positions, for instance, the outer thiophene units that may have potential electronic communications with the end groups (like non-covalent interactions between Se and O) and induce compact intermolecular packing. Moreover, incorporating more Se atoms into the molecular backbone, i.e., substitution at the benzothiadiazole and thienothiophene moieties simultaneously, would further extend the absorption range and narrower the bandgap due to enhanced quinoidal character of the acceptor. It is anticipated that these Se-based SMAs are desirable for ternary, semi-transparent and tandem solar cells, which could be promising to boost the efficiencies of these devices.

## Notes

The authors declare no competing financial interests.

## Acknowledgements

The work described in this paper was partially supported by the Shen Zhen Technology and Innovation Commission (project number JCYJ20170413173814007, JCYJ20170818113905024), the Hong Kong Research Grants Council (Research

Impact Fund R6021-18, project numbers 16305915, 16322416, 606012, and 16303917), Hong Kong Innovation and Technology Commission for the support through projects ITC-CNERC14SC01 and ITS/471/18), National Natural Science Foundation of China (NSFC, No. 91433202) and the National Key Research and Development Program of China (No. 2019YFA0705900) funded by MOST. X-ray data acquisition and manuscript input by NCSU authors are supported by ONR grant N000141712204 and N000142012155. X-ray data were acquired at the Advanced Light Source, which was supported by the Director, Office of Science, Office of Basic Energy Sciences, of the U.S. Department of Energy under Contract DE-AC02-05CH11231.

## References

- 1 G. Zhang, J. Zhao, P. C. Y. Chow, K. Jiang, J. Zhang, Z. Zhu, J. Zhang, F. Huang, H. Yan, *Chem. Rev.* 2018, **118**, 3447.
- 2 J. Q. Zhang, H. S. Tan, X. G. Guo, A. Facchetti, H. Yan, *Nat. Energy* 2018, **3**, 720.
- 3 J. Hou, O. Inganäs, R. H. Friend, F. Gao, *Nat. Mater.* 2018, **17**, 119.
- 4 C. Yan, S. Barlow, Z. Wang, H. Yan, A. K. Y. Jen, S. R. Marder, X. Zhan, *Nat. Rev. Mater.* 2018, **3**, 18003.
- 5 P. Cheng, G. Li, X. W. Zhan, Y. Yang, *Nat. Photon.* 2018, **12**, 131.
- 6 A. Wadsworth, M. Moser, A. Marks, M. S. Little, N. Gasparini, C. J. Brabec, D. Baran, I. McCulloch, *Chem Soc Rev* 2019, **48**, 1596.
- 7 Y. Tong, Z. Xiao, X. Du, C. Zuo, Y. Li, M. Lv, Y. Yuan, C. Yi, F. Hao, Y. Hua, T. Lei, Q. Lin, K. Sun, D. Zhao, C. Duan, X. Shao, W. Li, H.-L. Yip, Z. Xiao, B. Zhang, Q. Bian, Y. Cheng, S. Liu, M. Cheng, Z. Jin, S. Yang, L. Ding, *Sci China Chem* 2020, **63**, 758.8 Y. Lin, J. Wang, Z. G. Zhang, H. Bai, Y. Li, D. Zhu and X. Zhan, *Adv. Mater.*, 2015, **27**, 1170.
- 9 W. Zhao, S. Li, H. Yao, S. Zhang, Y. Zhang, B. Yang and J. Hou, *J. Am. Chem. Soc.*, 2017, **139**, 7148.

- 10 T. Jia, J. Zhang, W. Zhong, Y. Liang, K. Zhang, S. Dong, L. Ying, F. Liu, X. Wang, F. Huang and Y. Cao, *Nano Energy*, 2020, **72**, 104718.
- 11 Q. P. Fan, W. Y. Su, S. S. Chen, W. Kim, X. B. Chen, B. Lee, T. Liu, U. A. Mendez-Romero, R. J. Ma, T. Yang, W. L. Zhuang, Y. Li, Y. W. Li, T. S. Kim, L. T. Hou, C. Yang, H. Yan, D. H. Yu and E. G. Wang, *Joule*, 2020, **4**, 658.
- 12 J. Sun, X. Ma, Z. Zhang, J. Yu, J. Zhou, X. Yin, L. Yang, R. Geng, R. Zhu, F. Zhang and W. Tang, *Adv. Mater.*, 2018, **30**, e1707150.
- 13 B. Kan, H. Feng, X. Wan, F. Liu, X. Ke, Y. Wang, Y. Wang, H. Zhang, C. Li, J. Hou and Y. Chen, *J. Am. Chem. Soc.*, 2017, **139**, 4929.
- 14 Z. Yao, X. Liao, K. Gao, F. Lin, X. Xu, X. Shi, L. Zuo, F. Liu, Y. Chen and A. K. Jen, *J. Am. Chem. Soc.*, 2018, **140**, 2054.
- 15 Z. G. Zhang, Y. Yang, J. Yao, L. Xue, S. Chen, X. Li, W. Morrison, C. Yang and Y. Li, *Angew. Chem., Int. Ed. Engl.*, 2017, **56**, 13503.
- 16 H. Huang, Q. Guo, S. Feng, C. Zhang, Z. Bi, W. Xue, J. Yang, J. Song, C. Li, X. Xu, Z. Tang, W. Ma and Z. Bo, *Nat. Commun.*, 2019, **10**, 3038.
- 17 Z. Xiao, X. Jia, D. Li, S. Wang, X. Geng, F. Liu, J. Chen, S. Yang, T. P. Russell and L. Ding, *Sci. Bull.*, 2017, **62**, 1494.
- 18 Y. Li, H. Meng, T. Liu, Y. Xiao, Z. Tang, B. Pang, Y. Li, Y. Xiang, G. Zhang, X. Lu, G. Yu, H. Yan, C. Zhan, J. Huang and J. Yao, *Adv. Mater.*, 2019, **31**, e1904585.
- 19 J. Song, C. Li, L. Zhu, J. Guo, J. Xu, X. Zhang, K. Weng, K. Zhang, J. Min, X. Hao, Y. Zhang, F. Liu and Y. Sun, *Adv. Mater.*, 2019, **31**, e1905645.
- 20 N. Gasparini, S. H. K. Paleti, J. Bertrandie, G. Cai, G. Zhang, A. Wadsworth, X. Lu, H.-L. Yip, I. McCulloch and D. Baran, *ACS Energy Lett.*, 2020, **5**, 1371.
- 21 J. Gao, W. Gao, X. Ma, Z. Hu, C. Xu, X. Wang, Q. An, C. Yang, X. Zhang and F. Zhang, *Energy Environ. Sci.*, 2020, **13**, 958.
- 22 T. Liu, R. Ma, Z. Luo, Y. Guo, G. Zhang, Y. Xiao, T. Yang, Y. Chen, G. Li, Y. Yi, X. Lu, H. Yan and B. Tang, *Energy Environ. Sci.* 2020, DOI: 10.1039/d0ee00662a.
- 23 W. Yang, Z. Luo, R. Sun, J. Guo, T. Wang, Y. Wu, W. Wang, J. Guo, Q. Wu, M.

- Shi, H. Li, C. Yang and J. Min, *Nat. Commun.*, 2020, **11**, 1218.
- 24 L. L. Zhan, S. X. Li, T. K. Lau, Y. Cui, X. H. Lu, M. M. Shi, C. Z. Li, H. Y. Li, J. H. Hou and H. Z. Chen, *Energy Environ. Sci.*, 2020, **13**, 635.
- 25 X. Ma, J. Wang, J. Gao, Z. Hu, C. Xu, X. Zhang and F. Zhang, *Adv. Energy Mater.* 2020, **10**, 2001404.
- 26 Z. Hu, Z. Wang, Q. An and F. Zhang, *Sci. Bull.* 2020, **65**, 131.
- 27 J. Gao, J. Wang, Q. An, X. Ma, Z. Hu, C. Xu, X. Zhang and F. Zhang, *Sci China Chem*, 2020, **63**, 83-91.
- 28 S. Li, C.-Z. Li, M. Shi and H. Chen, *ACS Energy Lett.*, 2020, **5**, 1554.
- 29 J. Yuan, Y. Zhang, L. Zhou, G. Zhang, H.-L. Yip, T.-K. Lau, X. Lu, C. Zhu, H. Peng, P. A. Johnson, M. Leclerc, Y. Cao, J. Ulanski, Y. Li and Y. Zou, *Joule*, 2019, **3**, 1140.
- 30 C. Duan and L. Ding, *Sci. Bull.*, 2020, DOI: 10.1016/j.scib.2020.05.023.
- 31 L. Liu, Y. Kan, K. Gao, J. Wang, M. Zhao, H. Chen, C. Zhao, T. Jiu, A. K. Jen and Y. Li, *Adv. Mater.*, 2020, **32**, e1907604.
- 32 X. Du, Y. Yuan, L. Zhou, H. Lin, C. Zheng, J. Luo, Z. Chen, S. Tao, L. S. Liao and *Adv. Funct. Mater.*, 2020, **30**, 1909837.
- 33 Q. Liu, Y. Jiang, K. Jin, J. Qin, J. Xu, W. Li, J. Xiong, J. Liu, Z. Xiao, K. Sun, S. Yang, X. Zhang and L. Ding, *Sci. Bull.*, 2020, **65**, 272.
- 34 T. Wang, R. Sun, M. Shi, F. Pan, Z. Hu, F. Huang, Y. Li and J. Min, *Adv. Energy Mater.*, 2020, 2000590.
- 35 Z. Luo, R. Ma, T. Liu, J. Yu, Y. Xiao, R. Sun, G. Xie, J. Yuan, Y. Chen, K. Chen, G. Chai, H. Sun, J. Min, J. Zhang, Y. Zou, C. Yang, X. Lu, F. Gao and H. Yan, *Joule*, 2020 DOI: 10.1016/j.joule.2020.03.023.
- 36 J. Yuan, T. Huang, P. Cheng, Y. Zou, H. Zhang, J. L. Yang, S. Y. Chang, Z. Zhang, W. Huang, R. Wang, D. Meng, F. Gao and Y. Yang, *Nat. Commun.*, 2019, **10**, 570.
- 37 S. Li, L. Zhan, Y. Jin, G. Zhou, T. K. Lau, R. Qin, M. Shi, C. Z. Li, H. Zhu, X. Lu, F. Zhang and H. Chen, *Adv. Mater.*, 2020, e2001160.

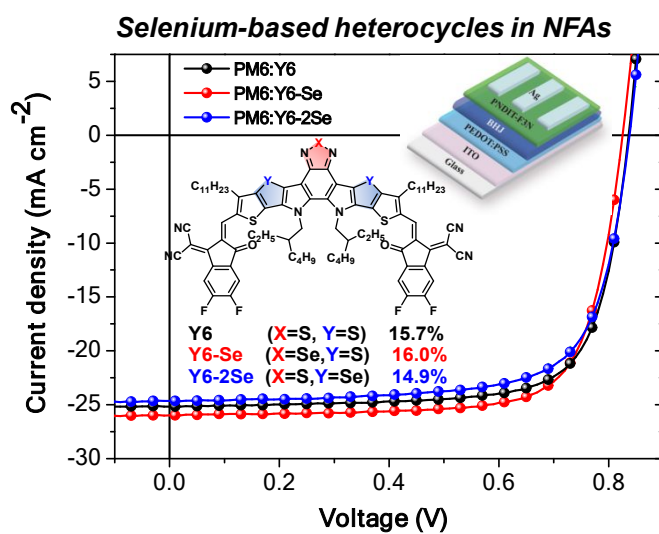
- 38 X. Xu, K. Feng, Y. W. Lee, H. Y. Woo, G. Zhang and Q. Peng, *Adv. Funct. Mater.*, 2020, **30**, 1907570.
- 39 Z. Zhou, W. Liu, G. Zhou, M. Zhang, D. Qian, J. Zhang, S. Chen, S. Xu, C. Yang, F. Gao, H. Zhu, F. Liu and X. Zhu, *Adv. Mater.*, 2020, **32**, e1906324.
- 40 R. Wang, J. Yuan, R. Wang, G. Han, T. Huang, W. Huang, J. Xue, H. C. Wang, C. Zhang, C. Zhu, P. Cheng, D. Meng, Y. Yi, K. H. Wei, Y. Zou and Y. Yang, *Adv. Mater.*, 2019, **31**, e1904215.
- 41 T. Liu, Y. Zhang, Y. Shao, R. Ma, Z. Luo, Y. Xiao, T. Yang, X. Lu, Z. Yuan, H. Yan, Y. Chen and Y. Li, *Adv. Funct. Mater.*, 2020, 2000456.
- 42 C. Sun, S. Qin, R. Wang, S. Chen, F. Pan, B. Qiu, Z. Shang, L. Meng, C. Zhang, M. Xiao, C. Yang and Y. Li, *J. Am. Chem. Soc.*, 2020, **142**, 1465.
- 43 H. Lai, Q. Zhao, Z. Chen, H. Chen, P. Chao, Y. Zhu, Y. Lang, N. Zhen, D. Mo, Y. Zhang and F. He, *Joule*, 2020, **4**, 688.
- 44 H. Wang, T. Liu, J. Zhou, D. Mo, L. Han, H. Lai, H. Chen, N. Zheng, Y. Zhu, Z. Xie and F. He, *Adv. Sci. (Weinh)*, 2020, **7**, 1903784.
- 45 H. Yu, R. Ma, Y. Xiao, J. Zhang, T. Liu, Z. Luo, Y. Chen, F. Bai, X. Lu, H. Yan and H. Lin *Mater. Chem. Front.*, 2020 DOI: 10.1039/D0QM00151A.
- 46 C. Huang, X. Liao, K. Gao, L. Zuo, F. Lin, X. Shi, C.-Z. Li, H. Liu, X. Li, F. Liu, Y. Chen, H. Chen and A. K.-Y. Jen, *Chem. Mater.*, 2018, **30**, 5429–5434.
- 47 T. Li, S. Dai, Z. Ke, L. Yang, J. Wang, C. Yan, W. Ma and X. Zhan, *Adv. Mater.*, 2018, **30**, 1705969.
- 48 Y. Li, J.-D. Lin, X. Che, Y. Qu, F. Liu, L.-S. Liao and S.-R. Forrest, *J. Am. Chem. Soc.*, 2017, **139**, 17114–17119.
- 49 J. Chen, G. Li, Q. Zhu, X. Guo, Q. Fan, W. Ma and M. Zhang, *J. Mater. Chem. A*, 2019, **7**, 3745–3751.
- 50 Z. Xiao, S. Yang, Z. Yang, J. Yang, H.-L. Yip, F. Zhang, F. He, T. Wang, J. Wang, Y. Yuan, H. Yang, M. Wang and L. Ding, *Adv. Mater.*, 2018, **30**, 1804790.
- 51 H. Yu, Z. Qi, X. Li, Z. Wang, W. Zhou, H. Ade, H. Yan and K. Chen, *Sol. RRL.*,

- 2020 DOI: 10.1002/solr.202000421.
- 52 J.-L. Wang, K.-K. Liu, L. Hong, G.-Y. Ge, C. Zhang and J. Hou, *ACS Energy Lett.*, 2018, **3**, 2967–2976.
- 53 Y. Li, L. Zhong, F.-P. Wu, Y. Yuan, H.-J. Bin, Z.-Q. Jiang, Z. Zhang, Z.-G. Zhang, Y. Li and L.-S. Liao, *Energy Environ. Sci.*, 2016, **9**, 3429–3435.
- 54 Z. Liang, M. Li, X. Zhang, Q. Wang, Y. Jiang, H. Tian and Y. Geng, *J. Mater. Chem. A*, 2018, **6**, 8059–8067.
- 55 C. Li, T. Xia, J. Song, H. Fu, H. S. Ryu, K. Weng, L. Ye, H. Y. Woo and Y. Sun, *J. Mater. Chem. A*, 2019, **7**, 1435–1441.
- 56 X. Liao, X. Shi, M. Zhang, K. Gao, L. Zuo, F. Liu, Y. Chen and A. K.-Y. Jen, *Chem. Commun.*, 2019, **55**, 8258–8261.
- 57 J. F. Van Humbeck, T. M. McDonald, X. Jing, B. M. Wiers, G. Zhu and J. R. Long, *J. Am. Chem. Soc.*, 2014, *136*, 2432–2440.
- 58 S. Holliday, R. S. Ashraf, A. Wadsworth, D. Baran, S. A. Yousaf, C. B. Nielsen, C.-H. Tan, S. D. Dimitrov, Z. Shang, N. Gasparini, M. Alamoudi, F. Laquai, C. J. Brabec, A. Salleo, J. R. Durrant and I. McCulloch, *Nat. Commun.*, 2016, **7**, 11585–11595.
- 59 C. E. Tsai, R. H. Yu, F. J. Lin, Y.-Y. Lai, J.-Y. Hsu, S. W. Cheng, C. S. Hsu and Y. J. Cheng, *Chem. Mater.*, 2016, **28**, 5121–5130.
- 60 B. Kim, H. R. Yeom, M. H. Yun, J. Y. Kim and C. Yang, *Macromolecules*, 2012, **45**, 8658–8664.
- 61 L. Zhong, H. Bin, I. Angunawela, Z. Jia, B. Qiu, C. Sun, X. Li, Z. Zhang, H. Ade and Y. Li, *Macromolecules*, 2019, **52**, 4776–4784.
- 62 S. P. Mishra, A. E. Javier, R. Zhang, J. Liu, J. A. Belot, I. Osaka and R. D. McCullough, *J. Mater. Chem.*, 2011, **21**, 1551–1561.
- 63 W. Zhang, J. Huang, J. Xu, M. Han, D. Su, N. Wu, C. Zhang, A. Xu and C. Zhan, *Adv. Energy Mater.* 2020, *10*, 2001436.
- 64 K.-K. Liu, X. Xu, J.-L. Wang, C. Zhang, G.-Y. Ge, F.-D. Zhuang, H.-J. Zhang, C.

- Yang, Q. Peng and J. Pei, *J. Mater. Chem. A*, 2019, **7**, 24389.
- 65 S.-S. Wan, X. Xu, J.-L. Wang, G.-Z. Yuan, Z. Jiang, G.-Y. Ge, H.-R. Bai, Z. Li and Q. Peng, *J. Mater. Chem. A*, 2019, **7**, 11802.
- 66 S.-S. Wan, X. Xu, Z. Jiang, J. Yuan, A. Mahmood, G.-Z. Yuan, K.-K. Liu, W. Ma, Q. Peng and J.-L. Wang, *J. Mater. Chem. A*, 2020, **8**, 4856.
- 67 J.-W. Lee, M. J. Sung, D. Kim, S. Lee, H. You, F. S. Kim, Y.-H. Kim, B. J. Kim and S.-K. Kwon, *Chem. Mater.*, 2020, **32**, 2572.
- 68 F. Lin, L. Zuo, K. Gao, M. Zhang, S. B. Jo, F. Liu and A. K. Y. Jen, *Chem. Mater.*, 2019, **31**, 6770.
- 69 Y. Chang, T.-K. Lau, P. C. Y. Chow, N. Wu, D. Su, W. Zhang, H. Meng, C. Ma, T. Liu, X. Zou, K. S. Wong, X. Lu, H. Yan and C. Zhan, *J. Mater. Chem. A*, 2020, **8**, 3676-3685.
- 70 V. V. Brus, C. M. Proctor, N. A. Ran and T.-Q. Nguyen, *Adv. Energy Mater.* 2016, **6**, 1502250.
- 71 H. Yu, L. Arunagiri, L. Zhang, J. Huang, W. Ma, J. Zhang and H. Yan, *J. Mater. Chem. A*, 2020, **8**, 6501-6509.
- 72 E. Gann, A. T. Young, B. A. Collins, H. Yan, J. Nasiatka, H. A. Padmore, H. Ade, A. Hexemer and C. Wang, *Rev. Sci. Instrum.*, 2012, **83**, 045110.
- 73 B. A. Collins, Z. Li, J. R. Tumbleston, E. Gann, C. R. McNeill and H. Ade, *Adv. Energy Mater.*, 2013, **3**, 65.
- 74 L. Ye, H. Hu, M. Ghasemi, T. Wang, B.A. Collins, J. H. Kim, K. Jiang, J. H. Carpenter, H. Li, Z. Li, T. McAfee, J. Zhao, X. Chen, J. L. Y. Lai, T. Ma, J. L. Bredas, H. Yan and H. Ade, *Nature Mater.*, 2018, **17**, 253–260.
- 75 A. Karki, J. Vollbrecht, A. L. Dixon, N. Schopp, M. Schrock, G. N. M. Reddy and T.-Q. Nguyen, *Adv. Mater.* 2019, **31**, 1903868.
- 76 H. Sun, H. Yu, Y. Shi, J. Yu, Z. Peng, X. Zhang, B. Liu, J. Wang, R. Singh, J. Lee, Y. Li, Z. Wei, Q. Liao, Z. Kan, L. Ye, H. Yan, F. Gao and X. Guo, *Adv. Mater.* 2020, DOI: 10.1002/adma.202004183.

- 77 H. Yao, L.-K. Ma, H. Yu, J. Yu, P. C. Y. Chow, W. Xue, X. Zou, Y. Chen, J. Liang, L. Arunagiri, F. Gao, H. Sun, G. Zhang, W. Ma and H. Yan, *Adv. Energy Mater.* 2020, DOI: 10.1002/aenm.202001408.
- 78 D. Qian, Z. Zheng, H. Yao, W.g Tress, T. R. Hopper, S. Chen, S. Li, J. Liu, S. Chen, J. Zhang, X.-K. Liu, B. Gao, L. Ouyang, Y. Jin, G. Pozina, I. A. Buyanova, W. M. Chen, O. Inganäs, V. Coropceanu, J.-L. Bredas, H. Yan, J. Hou, F. Zhang, A. A. Bakulin, Feng Gao, *Nature Mater.* 2018, **17**, 703.

## TOC graph



The selenium substitution strategy was applied to developed two new A'-DAD-A'-type small molecular acceptors. The resulting selenium-incorporated molecules exhibit red-shifted absorption and enhanced photon response, leading to high device efficiencies of over 16%.